

KLASS – The Role of Low-Mass Galaxies from Cosmic Dawn to Cosmic Noon

Adriano Fontana¹
 Charlotte A. Mason^{2,3}
 Marianne Girard⁴
 Tommaso Treu²
 Tucker Jones⁵
 Miroslava Dessauges-Zavadsky⁴
 Takahiro Morishita⁶
 Laura Pentericci¹
 Kasper Schmidt⁷
 Xin Wang²

¹ INAF, Osservatorio Astronomico di Roma, Italy

² Department of Physics and Astronomy, University of California, Los Angeles, USA

³ Harvard Smithsonian Center for Astrophysics, Cambridge, USA

⁴ Observatoire de Genève, Université de Genève, Switzerland.

⁵ Department of Physics, University of California, Davis, USA

⁶ Space Telescope Science Institute, Baltimore, USA

⁷ Leibniz-Institut für Astrophysik Potsdam, Potsdam, Germany

The KMOS Lens-Amplified Spectroscopic Survey (KLASS) is an ESO Large Programme that uses the KMOS infrared spectrograph to investigate the role of low-mass galaxies at several epochs of cosmic time. KLASS has targeted galaxies behind massive clusters, using gravitational amplification and stretching to observe galaxies that are intrinsically very faint. By pushing KMOS to the limits of its capabilities, we have obtained new constraints on the timescale of the reionisation process, finding that the intergalactic medium was almost completely neutral at a redshift of around 8, and that turbulence plays a major role in shaping low mass galaxies at intermediate redshifts ($0.5 < z < 2$).

In the first billion years of the Universe's life — the Cosmic Dawn — low-mass galaxies were the dominant population and their stellar emission was dominated by massive, short-lived, bright stars. Ultraviolet photons created by these stars were likely responsible for the most important transition that the Universe underwent after recombination: the reionisation of the intergalactic medium (IGM).

The bulk of this process occurred at redshifts $z > 7$, and coverage of this parameter space by spectroscopic surveys is still sparse and incomplete.

At lower redshifts ($0.5 < z < 2$), low-mass galaxies played a significant role in the evolution of the global star formation rate density, and they eventually contributed to the growth of more massive galaxies by merging processes. Feedback processes are much more effective in low-mass galaxies, as the energy release from supernovae and other feedback sources can exceed the gravitational binding energy. We thus expect the dynamical, morphological, dust and metallicity evolution in low-mass galaxies to be significantly different compared to their more massive siblings.

KLASS scientific goals

KLASS is designed to exploit the magnification due to gravitational lensing by massive clusters to observe (background) sources that are intrinsically much fainter than objects we can observe in ordinary fields; the image stretching in angular extent increases the spatial resolution. Our targets are galaxies that are gravitationally lensed by six massive galaxy clusters, four of which are among the well-known Frontier Fields¹. These are clusters that were previously observed by the large Hubble Space Telescope (HST) grism programme called the Grism Lens-Amplified Survey from Space (GLASS), which was led by Tommaso Treu. GLASS observed ten clusters with a wide set of spectroscopic observations. Capitalising on the magnification of background sources we were able to explore a range of redshifts and intrinsic magnitudes at a superior depth and quality than in blank fields located near the clusters — an exciting preview of JWST- and ELT-class science.

We have focused on two main scientific goals that are well-suited to the number of targets we can identify behind each cluster and to the number of integral field units (IFUs) in the *K*-band Multi-Object Spectrograph (KMOS):

1. To investigate Lyman alpha ($\text{Ly}\alpha$) emission from star-forming galaxies at redshifts $z > 7$ independently of HST

spectroscopic observations, providing validation and cross-calibration of HST results and enabling us to constrain the timeline of reionisation.

2. To probe the internal kinematics of galaxies at $z \sim 1-3$ with superior spatial resolution compared to surveys in blank fields.

KLASS observations were carried out by KMOS in the *YJ* bands (1–1.35 μm). The spectral resolution $R \sim 3400$ is sufficient to distinguish $\text{Ly}\alpha$ from potential low-redshift contaminants with the [OII] $\lambda 3726$, 3729 emission doublet at $z \sim 2$.

Observations were carried out in Service Mode and executed in one-hour observing blocks with repeating A-B-A integration corresponding to science-sky-science observations. Each observing block comprised 1800 s of science integration, and 900 s on sky. Exposure times ranged between approximately 6.5 and 15 hours per target. Dither shifts were included, shifting the pointing between science frames. A star was observed in one IFU in every observing block to monitor the point spread function (PSF) and the accuracy of dither offsets. The PSF was well-described by a circular Gaussian and the median seeing of our observations was 0.6 arcseconds.

Reaching the limits of KMOS: optimising the pipeline

To reach the ambitious goals of the KLASS survey it was necessary to squeeze the most out of our data. Observations of faint $\text{Ly}\alpha$ emission, comprising half of our sample, are challenging. The main difficulties that we have had to overcome are:

1. high-redshift candidates are not detected in the continuum with KMOS, so we cannot rely on a robust identification of their position in the spaxel space;
2. we need to subtract the background reliably to reach Poisson sensitivity limits;
3. we need to identify subtle systematics that can lead to spurious identifications of faint lines;
4. we need to quantify exactly the signal-to-noise ratio (S/N) achieved for each pixel of the extracted spectra in order

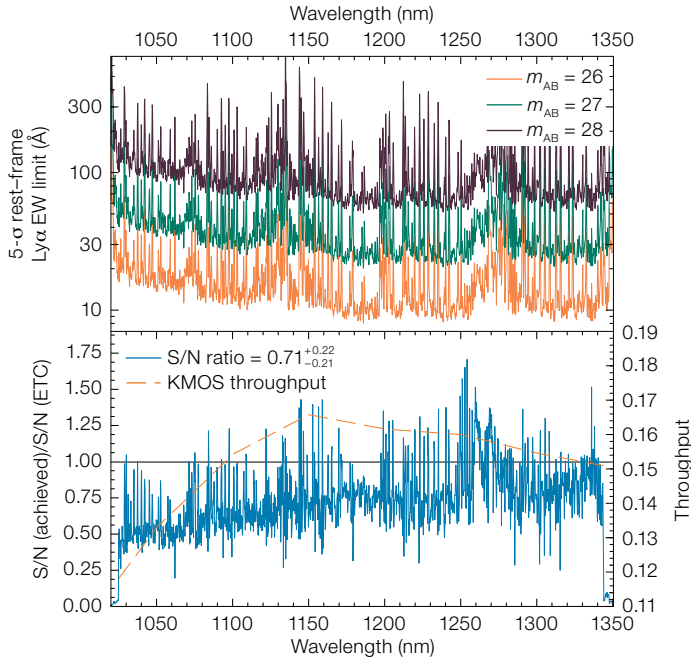


Figure 1. Upper: $5\text{-}\sigma$ rest-frame equivalent width limits in $\text{Ly}\alpha$ as a function of wavelength for three values of the apparent magnitude m in the ultraviolet. Lower: Comparison of the achieved sensitivity as a function of wavelength in our deepest exposure with the KMOS exposure time calculator using the same exposure times.

to evaluate the significance of faint lines or to statistically analyse the significance of non-detections, as described below.

To reach our goals we have extensively tailored, optimised and characterised the ESO pipeline (v1.4.3). Details of these improvements are given in Mason et al. (2019), to which we refer the reader. An example of the outcome of our efforts is given in Figure 1 (upper panel), in which we show the effective $5\text{-}\sigma$ rest-frame equivalent width (EW) limits in $\text{Ly}\alpha$ as a function of wavelength for three values of apparent magnitude in the ultraviolet, assuming emission lines are spatially unresolved. It is clear that the sensitivity changes dramatically with variability in the sky emission lines, ubiquitous in the near-infrared, and their effect needs to be factored into the estimate of the survey efficiency.

Another important lesson that we have learned from this exercise is shown in the lower panel of Figure 1, where we compare the observed S/N with that predicted by the ESO exposure time calculator (ETC). We find that, owing to inevitable systematics in sky subtraction, the predicted S/N was about 1.5 times higher than that observed. Future observers are strongly advised to include this factor in their predictions.

Armed with this careful characterisation of the instrument, we have used our data to explore two hot topics in modern cosmology.

Cosmic dawn: which sources reionised the early Universe?

The reionisation of intergalactic hydrogen in the Universe’s first billion years is likely linked to the formation of the first stars and galaxies, considered to be the primary producers of hydrogen-ionising photons. Accurately measuring the time-line of reionisation enables us to constrain the properties of these first sources.

Whilst young star-forming galaxies show $\text{Ly}\alpha$ emission (121.6 nm) in increasing abundance at higher redshifts up to $z \sim 6$, the fraction of galaxies detected with $\text{Ly}\alpha$ emission, and the equivalent width distribution of that emission, decreases rapidly (for example, Fontana et al., 2010; Pentericci et al., 2018 and references therein). This rapid decline of detected $\text{Ly}\alpha$ emission is unlikely to be due to the physical evolution of the galaxy properties, as we expect the trend toward stronger $\text{Ly}\alpha$ to continue at higher redshifts because of decreasing metallicity and dust content. The decline is most plausibly due to absorption in an increas-

ingly neutral IGM, which progressively absorbs the intrinsic $\text{Ly}\alpha$ emission. The drop in the $\text{Ly}\alpha$ EW distribution at $z \sim 7$ yields the best current constraint on the mid-stages of the reionisation process (Mason et al., 2018).

By targeting galaxy candidates at $z \sim 8$, KLASS had the explicit aim of extending this analysis to higher redshifts, in order to trace the reionisation process at its peak, when newborn galaxies were producing sufficient ultraviolet photons to significantly ionise the IGM. The choice of an IFU instrument for high-redshift $\text{Ly}\alpha$ observations was motivated by indications that ground-based slit spectroscopy measures lower $\text{Ly}\alpha$ flux than HST slitless grism spectroscopy. As demonstrated by recent MUSE observations, $\text{Ly}\alpha$ emission can be spatially extended and/or offset from the ultraviolet continuum emission, making it likely that slit-based spectroscopy is not capturing the full $\text{Ly}\alpha$ flux. Hence, the observed decline in $\text{Ly}\alpha$ emission at $z > 6$ could be partially due to redshift-dependent slit-losses as well as reionisation.

The answer from KLASS is unambiguous: despite the high quality of the parent photometric sample based on the best HST images and the depth reached by the KMOS observations, none of the 29 galaxies with photometric redshifts of ~ 8 show significant $\text{Ly}\alpha$ emission. Crucially, our sample is composed of a sizeable fraction of intrinsically faint galaxies (thanks to the effect of gravitational lensing), which are most likely to have strong $\text{Ly}\alpha$ emission at lower redshifts.

Using sensitivity estimates as a function of wavelength for every target, we have defined a robust Bayesian scheme to derive the neutral hydrogen fraction of the IGM at $z \sim 8$. Our inference accounts for wavelength sensitivity, the incomplete redshift coverage of our observations, the photometric redshift probability distribution of each target, and the patchy nature of reionisation. The KLASS observations enable us to place the first robust lower limit on the average IGM neutral hydrogen fraction at $z \sim 8$ of > 0.76 (with 68% confidence), > 0.46 (95% confidence), providing crucial evidence of rapid reionisation at $z \sim 6\text{--}8$. This is shown in Figure 2, in which we compare the derived IGM neu-

tral fraction from KLASS with other constraints. We find that the fraction that we derive is consistent with reionisation history models that extend the galaxy luminosity function to $M_{UV} \lesssim -12$, with low ionising photon escape fractions, $f_{esc} \lesssim 15\%$.

We note that the lack of detected Ly α lines is not (only) due to the difficulty of performing efficient near-infrared spectroscopy. As a counter example, we have detected a faint C IV emission doublet from a known $z = 6.11$ galaxy, that we use to showcase the capability of KMOS to detect very faint emission lines. The resulting spectrum is shown in Figure 3. The emission lines are partly absorbed by a nearby sky emission line and have a total flux of the order of 10^{-17} erg s $^{-1}$ cm $^{-2}$.

Cosmic high noon: the dynamical state of low-mass galaxies.

The redshift range $1 < z < 3$ was the most active time in the Universe's history, covering the peak of cosmic star formation history when more than half of the stellar mass in the Universe was built up. Many galaxies at this epoch appear morphologically disordered; the clear bimodality in the galaxy population in the local Universe, between rotating discs and dispersion-dominated elliptical galaxies has not yet been established. How this bimodality arises and which processes change galaxies from discs to ellipticals are still open questions.

Using integral field spectroscopy, we can ask questions about how galaxy morphologies and kinematics are related to their past and ongoing star formation (for example, Förster Schreiber et al., 2009). A key question is whether the increase in star formation rates (SFRs) is driven solely by an increase in density and smooth gas accretion rates at higher redshifts producing steady in-situ star formation, or by more stochastic processes leading to gas infall such as major mergers.

The first generations of integral-field surveys using single IFU instruments (primarily SINFONI and GIRAFFE) as well as recent surveys using KMOS (for example, KMOS^{3D}, Wisnioski et al., 2015) have primarily targeted star-forming galaxies at the high mass end of the galaxy stellar

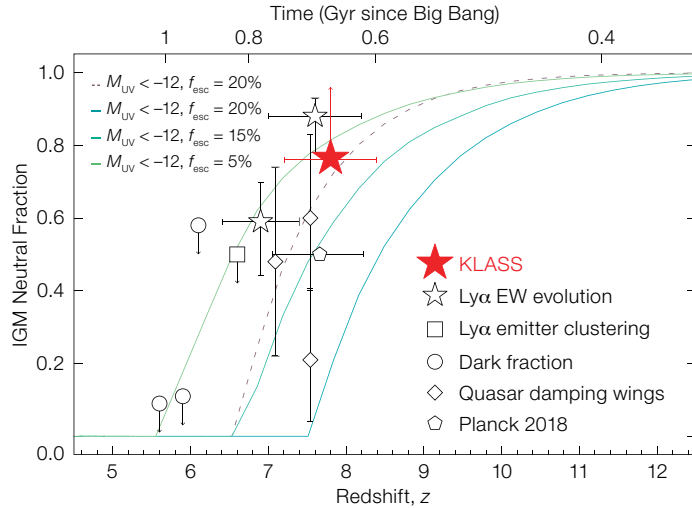


Figure 2. The evolution in redshift of the volume-averaged neutral hydrogen fraction of the IGM. The lower limit from KLASS is the highest-redshift star (shown in red).

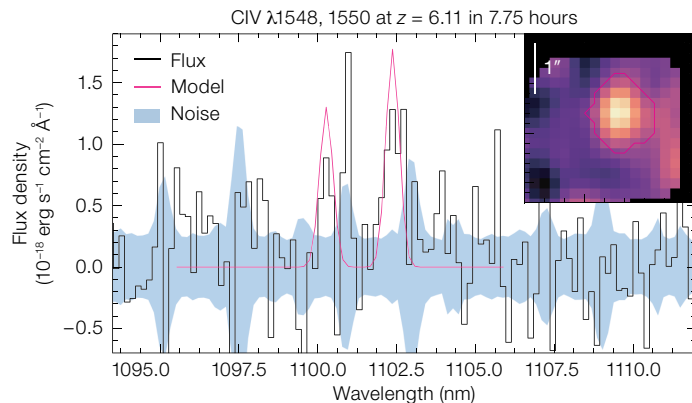


Figure 3. KMOS KLASS 1D spectrum and 2D emission-line map of the galaxy at $z = 6.11$, centred on the faint C IV doublet emission (in pink).

mass function ($\gtrsim 10^{10} M_{\odot}$). Most surveys found samples of $z \sim 1-3$ galaxies which were roughly equally separated into three kinematic classifications: rotation-dominated systems, dispersion-dominated systems and merging/morphologically unstable systems. A key result was that the rotation-dominated systems had systematically higher velocity dispersions than local discs, suggesting that high redshift discs are highly turbulent.

However, there is no clear picture of the kinematic evolution of low-mass galaxies. It is also known that seeing-limited observations can lead to the misclassification of these objects, the result of seeing-induced smearing of irregular rotational features in the spectra.

While adaptive-optics assisted observations are difficult and limited to small

samples, the combination of HST imaging, the amplification and size stretching due to gravitational lensing, and the multiplexing capability of KMOS makes it possible to study the internal motions of galaxies with low stellar masses in sizeable samples, and at higher spatial resolution than natural seeing (see Girard et al., 2018 for another example). This was the primary goal of the KLASS observations of intermediate-redshift galaxies.

In the KLASS survey we have observed 50 faint galaxies, spanning the mass range $7.7 < \log (M/M_{\odot}) < 10.8$. Observed redshifts span the range $0.6 < z < 2.3$, with 14 sources at $z > 1.5$ and two at $z > 2$.

For 42 of these galaxies we are able to obtain high-S/N kinematic maps. Some examples are shown in Figure 4, where we show the HST images, the 2D emis-

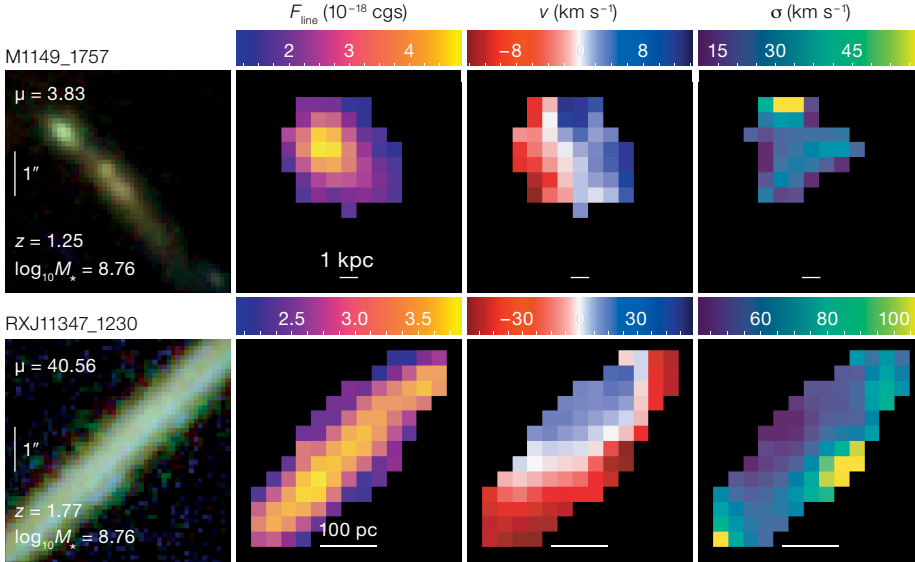


Figure 4. The HST *RGB* composite images, 2D emission-line spectra and velocity maps for two low-mass galaxies in KLASS.

pared to local discs and thus that the fraction of dynamically hot discs changes with cosmic time. Clearly, turbulence plays a major role in the settlement of rotating discs at low masses in the young Universe.

The power of KMOS has revealed once more the crucial role that faint, low-mass galaxies have had in the history of the Universe. They produced most of the ultraviolet photons required to reionise the Universe in the redshift range $z = 6-9$. They continued to develop during the peak of cosmic star-formation history, building stars in highly turbulent systems. The kinematic analysis of our full sample, which is under way at the moment, will help to complete the picture regarding these fascinating systems.

sion lines and the velocity maps (circular velocity and dispersion) for the lowest-mass galaxies in the sample.

The circular velocity v and the velocity dispersion σ are used to classify galaxies as “rotationally supported” when $v/\sigma > 1$. Large values of $v/\sigma > 3-5$ typically indicate “regular rotation”, while lower values indicate that the systems are dynamically hotter, with turbulence in the disc being significantly higher than in local discs.

We find that the majority (77%) of our kinematically resolved sample are rotationally supported, but about a half of the sample (16/34) show particularly low values of $v/\sigma < 3$, meaning that most of the rotation-dominated galaxies are only marginally stable, at odds with what we see in the local Universe. We also find a mean dispersion of $\sigma \sim 55 \text{ km s}^{-1}$ in the sample, similar to previous surveys at the same redshifts.

We also used the observed emission lines in KMOS ($H\alpha$ at $z < 1$, $H\beta$ at $1 \leq z < 1.8$ or $[OII]$ at $z \geq 1.8$) to estimate the ongoing SFR in our sample, and investigated correlations between rotational state, SFR and stellar mass. Results are shown in Figure 5, where we show how objects with different rotational classifications are located in the main sequence plane. While there is significant scatter, there is some evidence that merging and irregular systems have a rel-

atively large ratio of $SFR:M_*$ ($> 0.1 \text{ Gyr}^{-1}$) suggesting that their disturbed gas dynamics may be enhancing star formation (or vice versa) in some of these objects compared to kinematically ordered systems. We also find a strong correlation between the dispersion and the stellar mass and SFR, meaning that high dispersion could be due to stellar feedback in these galaxies. Full results are given in Mason et al. (2017) and Girard et al. (in preparation).

This indicates that turbulence in discs is significantly higher at cosmic noon com-

References

Förster Schreiber, N. et al. 2009, *ApJ*, 706, 1364
 Fontana, A. et al. 2010, *ApJL*, 725, 205
 Girard, M. et al. 2018, *A&A*, 613, 72
 Mason, C. A. et al. 2017, *ApJ*, 838, 14
 Mason, C. A. et al. 2018, *ApJ*, 856, 2
 Mason, C. A. et al. 2019, *MNRAS*, 485, 3947
 Pentericci, L. et al. 2018, *A&A*, 619, 147
 Wisnioski, E. et al. 2015, *ApJ*, 799, 209

Links

¹ HST Frontier Fields: <http://www.stsci.edu/hst/campaigns/frontier-fields/>

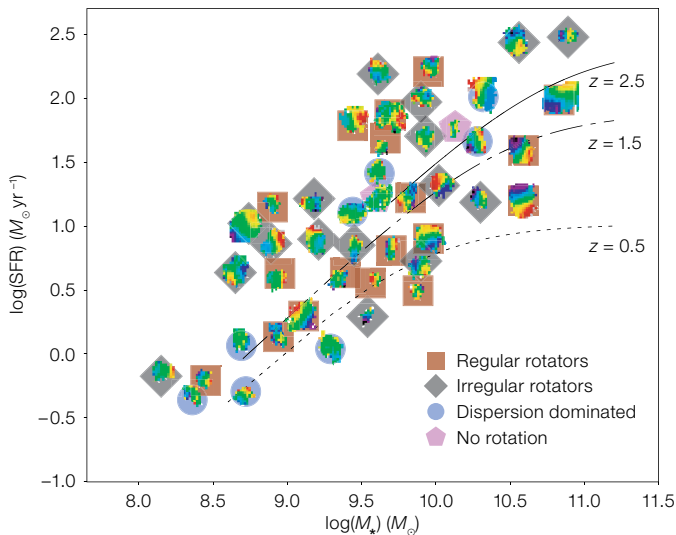


Figure 5. The velocity maps for galaxies in our sample with resolved kinematics, plotted at the galaxy’s position on the SFR– M_* plane.